

Article

Numerical Study of Efficient Tm-Doped Zinc-Tellurite Fiber Lasers at 2300 nm

Elena A. Anashkina *  and Alexey V. Andrianov

A.V. Gaponov-Grekhov Institute of Applied Physics of the Russian Academy of Sciences, 46 Ulyanov Street, 603950 Nizhny Novgorod, Russia

* Correspondence: elena.anashkina@ipfran.ru

Abstract: Fiber laser sources operating near 2300 nm in the atmospheric transparency window are interesting for different applications, such as remote sensing, lidars, and others. The use of Tm-doped fiber lasers based on tellurite fibers is highly promising. We propose and theoretically study a highly efficient diode-pumped Tm-doped zinc-tellurite fiber laser operating at two cascade radiative transitions at 1960 nm and 2300 nm, with additional energy transfer between these laser waves due to the Raman interaction. We demonstrate numerically that a dramatic increase in the slope efficiency up to 57% for the laser wave at 2300 nm, exceeding the Stokes limit by 22% relative to the pump at 793 nm, can be obtained with optimized parameters thanks to Raman energy transfer from the laser wave at 1960 nm to the wave at 2300 nm.

Keywords: tellurite glass fiber; Raman fiber laser; dual-wavelength lasers

1. Introduction

Laser sources around 2300 nm are needed for many applications, including the sensing of dangerous gases such as CO, HF, and CH₄. This wavelength belongs to the atmospheric transparency window, which is very attractive for many purposes. Therefore, the development of compact fiber laser sources of watt and ten-watt power levels is an important task today [1].

There are several ways to obtain coherent light at wavelengths near 2300 nm with compact optical fiber systems based on nonlinear light conversion [2–8], as well as on laser generation at a radiative transition of active ions [1,9–15]. One of them is supercontinuum generation in different nonlinear fibers [2–5]. Another solution is continuous-wave (CW) Raman lasers [6,7]. For example, a high-power CW Raman laser at 2350 nm based on undoped zinc-tellurite fibers with a 300 W pump at 2 μm was theoretically discussed in [8]. At the same time, fiber lasers with a standard diode pump at 793 nm, operating at the ³H₄ → ³H₅ transition of the Tm³⁺ ions, seem to be a rather promising and simpler solution. However, fibers based on silica glasses are not suitable for such lasers, due to their high phonon energy, so Tm:fluoride fibers [10–12] or Tm:tellurite fibers [13–16] are used. Nonetheless, it should be noted that Raman solitons at a wavelength of 2300 nm can also be obtained in Tm:silica fibers due to the soliton self-frequency shift [17–19], but not due to laser generation at the ³H₄ → ³H₅ transition (Tm:silica fiber lasers can be used to generate ultrashort pulses near 1900 nm [20], which can be further frequency-shifted due to the Raman effect). Obtaining high average powers (watt level) for Raman soliton sources seems to be a challenge. CW and quasi-CW lasers are a straightforward solution. Watt-level quasi-CW lasing with a high slope efficiency of 37% was obtained in a Tm:fluoride fiber laser pumped at 1.05 μm [11] (for the estimated Stokes limit of approximately 46%). To date, for Tm-doped zinc-tellurite fiber lasers operating near 2300 nm, the maximum experimentally achieved powers are a few hundred mW [15]. However, as we will show below, this is far from the limit. Moreover, due to an additional channel of energy transfer, the conversion efficiency of a 793 nm diode pump into a 2300 nm laser wave can, in principle, exceed



Citation: Anashkina, E.A.; Andrianov, A.V. Numerical Study of Efficient Tm-Doped Zinc-Tellurite Fiber Lasers at 2300 nm. *Fibers* **2023**, *11*, 57. <https://doi.org/10.3390/fib11070057>

Academic Editor: Walter Belardi

Received: 28 April 2023

Revised: 14 June 2023

Accepted: 21 June 2023

Published: 26 June 2023



Copyright: © 2023 by the authors. Licensee MDPI, Basel, Switzerland. This article is an open access article distributed under the terms and conditions of the Creative Commons Attribution (CC BY) license (<https://creativecommons.org/licenses/by/4.0/>).

the Stokes limit of $(793 \text{ nm}/2300 \text{ nm}) \times 100\% \sim 35\%$. Although we are not aware of any work where the slope efficiency around 2300 nm in Tm-doped lasers has exceeded the Stokes limit, such results are known for other lasers. For example, the exceedance of the Stokes limit was demonstrated in a Tm³⁺-doped silica fiber laser operating at $\sim 2 \mu\text{m}$ thanks to the cross-relaxation process [21]. Another example demonstrated experimentally is an Er:ZBLAN fiber laser at 2800 nm pumped at 976 nm with efficiency of $\sim 50\%$, which significantly exceeds the Stokes limit due to the effective use of the energy up-conversion process at dual-wavelength generation [22].

In this work, we propose and study numerically a highly efficient diode-pumped Tm-doped zinc-tellurite fiber laser operating at two cascade radiative transitions at 1960 nm and 2300 nm, with additional energy transfer between these laser waves due to the Raman interaction. We demonstrate numerically that a dramatic increase in the slope efficiency for the laser wave at 2300 nm, exceeding the Stokes limit relative to the pump at 793 nm, can be obtained using optimized parameters thanks to the Raman energy transfer from the laser wave at 1960 nm to the wave at 2300 nm. We note that the proposed idea is realizable mainly for the tellurite class of glasses, which have a huge width of the Raman gain band and a large value of the gain. For zinc-tellurite glasses, the maximum of the Raman gain is at ~ 22.5 THz, and its absolute value is almost 60 times higher than the maximum value for silica glass [23]. Note that the cascade laser amplification at 1960 nm and 2300 nm is chosen to maximize the Raman interaction between these wavelengths. For fluoride glasses, the conditions are worse: the gain maximum is at 17 THz, and its value is comparable to that for silica glass. For this reason, zinc-tellurite glass fibers are a promising active medium for lasers at 2300 nm with efficiency exceeding the Stokes limit due to additional Raman energy transfer between the laser waves generated in a cascade scheme at Tm³⁺ ion transitions.

2. Materials and Methods

A simplified scheme of energy levels of Tm³⁺ ions in a zinc-tellurite glass matrix providing dual-wavelength lasing at $\lambda_1 = 1960$ nm and $\lambda_2 = 2300$ nm, with a pump at $\lambda_p = 793$ nm, is presented in Figure 1a [14,24]. The scheme of the stimulated Raman process is shown in Figure 1b. Raman amplification at 2300 nm from the 1960 nm wave is most efficient, since the frequency difference between these wavelengths corresponds to a frequency of 22.5 THz of maximum Raman gain. Emission and absorption cross-sections of radiative transitions (based on the data from [14]) are plotted in Figure 1c. The model Raman gain function of zinc-tellurite glass in comparison with the Raman gain function of SiO₂ glass is plotted in Figure 1d (based on the data from [23]). The parameters describing the spectroscopic properties of Tm ions in the zinc-tellurite glass matrix are listed in Table 1. They are taken from our work [14] and from [24].

As a gain medium for highly efficient lasers, we considered a zinc-tellurite double-clad fiber having the following design. The diameter d of the Tm-doped core and the numerical aperture (NA) were chosen to provide single-mode propagation for both laser wavelengths. We set $d = 7 \mu\text{m}$ and $\text{NA} = 0.2$, providing a V parameter of 2.244 at 1960 nm and 1.912 at 2300 nm. The diameter of the first cladding where the pump propagated was $D = 70 \mu\text{m}$. The diameter of the second cladding was not important in our simulations. We assumed that the background optical losses could be 0.3 dB/m at 1960 and 2300 nm and 0.4 dB/m, which are attainable with modern technologies [25,26]. We considered the scheme of dual-wavelength laser generation presented in Figure 2. The reflection coefficients at the input ($z = 0$) and output ($z = L$) ends of the active fiber are $R_{01,02}$ and $R_{Lp,L1,L2}$, respectively. The subscript “p” corresponds to the pump wave and subscripts 1,2 to laser waves at 1960 nm and 2300 nm, respectively. The required selective reflection can be obtained using fiber Bragg gratings or selective mirrors. We assumed the reflection at the input end to be 99% for the laser waves and that at the output end to be 99% for the residual pump wave and the wave at 1.96 μm . We also assumed that the reflection could be changed for the target wave at 2300 nm. The losses at the input and output reflectors are 1% for all

waves. The radiation at 1960 nm is trapped in the resonator for efficient Raman interaction with the wave at 2300 nm.

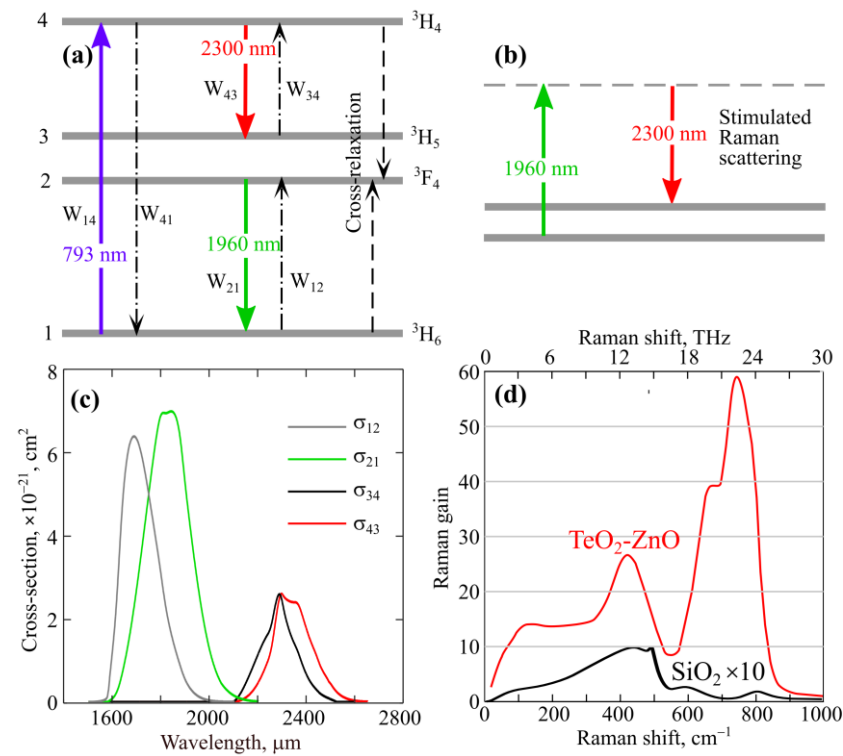


Figure 1. (a) Schematic representation of the energy levels of Tm^{3+} ions. (b) Schematic representation of stimulated Raman scattering. (c) Absorption and emission cross-sections of ${}^3H_4 \rightarrow {}^3H_5$ and ${}^3F_4 \rightarrow {}^3H_6$ radiative transitions. (d) Model Raman gain spectra of zinc-tellurite glass (red) and silica glass (multiplied by 10; black curve).

Table 1. Values for Tm-doped zinc-tellurite glass used in simulation describing pump and laser wavelengths, lifetimes of energy levels, branching ratios, absorption and emission cross-sections and cross-relaxation rates.

Parameter	Symbol	Value
Pump wavelength at $1 \rightarrow 4$ (${}^3H_6 \rightarrow {}^3H_4$) transition	λ_p	793 nm
Laser wavelength at $2 \rightarrow 1$ (${}^3F_4 \rightarrow {}^3H_6$) transition	λ_1	1960 nm
Laser wavelength at $4 \rightarrow 3$ (${}^3H_4 \rightarrow {}^3H_5$) transition	λ_2	2300 nm
Total lifetime of level 2 (3F_4)	τ_2	3 ms
Total (non-radiative) lifetime of level 3 (3H_5)	τ_3	0.13 μ s
Non-radiative lifetime of level 4 (3H_6)	τ_4^{NR}	1.2 ms
Radiative lifetime of level 4 (3H_6)	τ_4^R	0.4 ms
Total lifetime of level 4 (3H_6)	τ_4	0.3 ms
Branching ratio from level 4 to levels 3, 2, 1	β_{43}	0.03
	β_{42}	0.07
	β_{41}	0.09
Absorption cross-section at $1 \rightarrow 4$ transition	σ_{14}	1×10^{-20} cm ²
Emission cross-section at $4 \rightarrow 1$ transition	σ_{41}	1×10^{-20} cm ²
Absorption cross-section at $1 \rightarrow 2$ transition	σ_{12}	0.012×10^{-20} cm ²
Emission cross-section at $2 \rightarrow 1$ transition	σ_{21}	0.26×10^{-20} cm ²
Absorption cross-section at $3 \rightarrow 4$ transition	σ_{34}	0.26×10^{-20} cm ²
Emission cross-section at $4 \rightarrow 3$ transition	σ_{43}	0.26×10^{-20} cm ²
Cross-relaxation rate (for $N_{Tm} = 2 \times 10^{20}$ cm ⁻³)	K_{CR}	5678 s ⁻¹

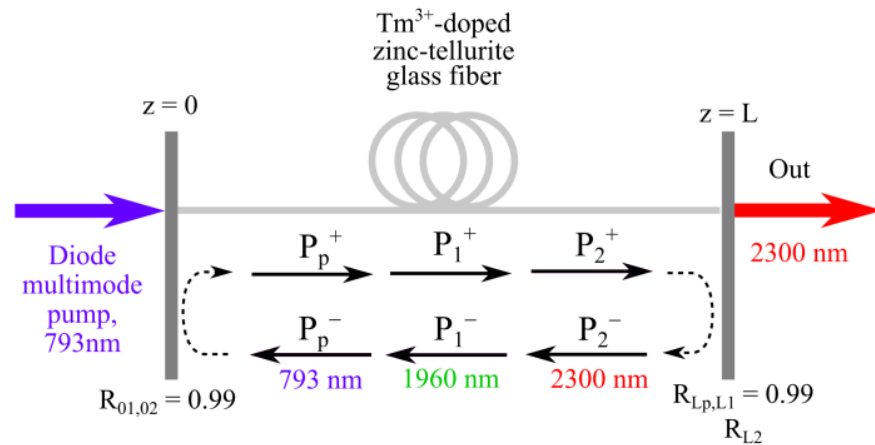


Figure 2. Schematic diagram of the laser setup based on Tm³⁺-doped zinc-tellurite glass fiber. R_{01} , R_{02} are the reflection coefficients at the input fiber end for waves at 1960 nm and 2300 nm, respectively. R_{L1} , R_{L2} and R_{Lp} are the reflection coefficients at the output fiber end for waves at 1960 nm, 2300 nm and 793 nm, respectively.

To simulate a dual-wavelength CW laser based on a double-clad Tm-doped zinc-tellurite fiber with high Raman gain, we generalized the previously developed numerical model for a dual-band Tm³⁺-doped tellurite fiber laser [14] with allowance for the Raman gain. In our previous work [14], we neglected the Raman effect, since it was irrelevant to the parameters of the experimental scheme. Here, we took into account rate equations for levels ³H₆, ³F₄, ³H₅ and ³H₄; Raman-modified equations for the evolution of the pump and signal waves along the z -axis; and boundary conditions. The rate equations with allowance for the cross-relaxation process (³H₄ + ³H₆ → ³F₄ + ³F₄) are written for the population densities n_1 , n_2 , n_3 and n_4 (with normalization to the concentration of Tm³⁺ ions in the core $N_{Tm} = 2 \times 10^{20} \text{ cm}^{-3}$) in the following form [14,24,27]:

$$\frac{\partial n_1}{\partial t} = -(W_{12} + W_{14})n_1 + \left(W_{21} + \frac{1}{\tau_2}\right)n_2 + \left(W_{41} + \frac{\beta_{41}}{\tau_4^R}\right)n_4 - K_{CR}n_4n_1 = 0 \quad (1)$$

$$\frac{\partial n_2}{\partial t} = W_{12}n_1 - \left(W_{21} + \frac{1}{\tau_2}\right)n_2 + \frac{n_3}{\tau_3} + \frac{\beta_{42}}{\tau_4^R}n_4 + 2K_{CR}n_4n_1 = 0 \quad (2)$$

$$\frac{\partial n_3}{\partial t} = -\left(W_{34} + \frac{1}{\tau_3}\right)n_3 + \left(W_{43} + \frac{\beta_{43}}{\tau_4^R} + \frac{1}{\tau_4^{NR}}\right)n_4 = 0 \quad (3)$$

$$n_1 + n_2 + n_3 + n_4 = 1, \quad (4)$$

where t is time; τ_2 and τ_3 are the total lifetimes of level 2 (³F₄) and level 3 (³H₅), respectively; τ_4^R and τ_4^{NR} are the radiative and non-radiative lifetimes of level 4 (³H₄) (the total lifetime of level 4 is $\tau_4 = (1/\tau_4^R + 1/\tau_4^{NR})^{-1}$); W_{ij} are the stimulated absorption (if $i < j$) or emission (if $i > j$) rates from level i to level j ; β_{43} , β_{42} and β_{41} are the branching ratios from level 4 to level 3, 2 and 1, respectively; and K_{CR} is the coefficient describing the cross-relaxation rate. The stimulated rates for the pump wave are

$$W_{14,41} = \frac{\Gamma_p \lambda_p \sigma_{14,41} (P_p^+ + P_p^-)}{hc A_c}, \quad (5)$$

where c is the speed of light in vacuum, the constant h is Planck's constant, σ_{41} and σ_{14} are the emission and absorption cross-sections at the pump wavelength λ_p , P_p^+ and P_p^- are the powers in the forward and backward waves at λ_p , A_c is the area of the Tm-doped core and Γ_p is the overlap integral of the pump distribution with the doped core evaluated as

$\Gamma_p = A_c/(\pi D^2/4)$. The stimulated emission rates (σ_{21} and σ_{43}) and absorption rates (σ_{12} and σ_{34}) for laser waves at wavelengths $\lambda_1 = 1960$ nm and $\lambda_2 = 2300$ nm are

$$W_{21,12} = \frac{\Gamma_1 \lambda_1 \sigma_{21,12} (P_1^+ + P_1^-)}{hc A_c} \quad (6)$$

$$W_{43,34} = \frac{\Gamma_2 \lambda_2 \sigma_{43,34} (P_2^+ + P_2^-)}{hc A_c}, \quad (7)$$

where Γ_1 and Γ_2 are the overlap integrals of the laser waves with the doped core, and $P_{1,2}^+$ and $P_{1,2}^-$ are the powers in the forward- and backward-propagating waves at $\lambda_{1,2}$.

The Raman-modified equations for the power evolution of the forward- and backward-propagating linearly polarized waves are constructed as [14,24,27–29]

$$\pm \frac{dP_p^\pm}{dz} = -\Gamma_p N_{Tm} (\sigma_{14} n_1 - \sigma_{41} n_4) P_p^\pm - \alpha_p P_p^\pm \quad (8)$$

$$\pm \frac{dP_1^\pm}{dz} = \Gamma_1 N_{Tm} (\sigma_{21} n_2 - \sigma_{12} n_1) P_1^\pm - g_{R12} \frac{\lambda_2}{\lambda_1} (P_2^+ + P_2^-) P_1^\pm - \alpha_1 P_1^\pm \quad (9)$$

$$\pm \frac{dP_2^\pm}{dz} = \Gamma_2 N_{Tm} (\sigma_{43} n_4 - \sigma_{34} n_3) P_2^\pm + g_{R12} (P_1^+ + P_1^-) P_2^\pm - \alpha_2 P_2^\pm \quad (10)$$

where $\alpha_{p,1,2}$ are the optical losses at $\lambda_{p,1,2}$, and g_{R12} is the coefficient describing the Raman gain from the wave at 1960 nm to the wave at 2300 nm in the zinc-tellurite fiber.

The Raman gain coefficient $g_{R12} = 5 \times 10^{-4}$ (W cm) $^{-1}$ for the zinc-tellurite glass fiber with the considered design was estimated as

$$g_{R12} = \frac{g_R(\text{TZ@1 } \mu\text{m}) \times (1 \mu\text{m}/\lambda_1)}{(A_{eff1} + A_{eff2})/2}. \quad (11)$$

Here, $g_R(\text{TZ@1 } \mu\text{m}) = 59 \times 10^{-13}$ m/W is the maximum Raman gain for bulk zinc-tellurite glass at 1 μm [23,28], and A_{eff1} and A_{eff2} are the effective mode field areas at 1960 nm and 2300 nm, respectively.

The boundary conditions for Equations (8)–(10) are written as

$$P_1^+(0) = R_{01} P_1^-(0) \quad (12)$$

$$P_1^-(L) = R_{L1} P_1^+(L) \quad (13)$$

$$P_2^+(0) = R_{02} P_2^-(0) \quad (14)$$

$$P_2^-(L) = R_{L2} P_2^+(L) \quad (15)$$

$$P_p^-(L) = R_{Lp} P_p^+(L), \quad (16)$$

and $P_p = P_p(0)$ is the pump power. We assumed that the losses for laser waves were 1% at each reflector at $z = 0$ and $z = L$. The output power at 2300 nm is $P_2^+(L) \times (1 - 0.01 - R_{L2})$.

All fiber parameters used in the simulations are listed in Table 2.

Table 2. Parameters used in simulations.

Parameter	Symbol	Value
Intracavity fiber length	L	30 ... 300 cm
Tm-doped core diameter	d	7 μm
Tm ion concentration in the core	N_{Tm}	$2 \times 10^{20} \text{ cm}^{-3}$
Numerical aperture (core/cladding)	NA	0.2
Cladding diameter	D	70 μm
Effective mode field area at $\lambda_1 = 1960 \text{ nm}$	A_{eff1}	51 μm^2
Effective mode field area at $\lambda_2 = 2300 \text{ nm}$	A_{eff2}	67 μm^2
Overlap integral (pump with doped area)	Γ_p	0.01
Overlap integral (1960 nm wave with doped core)	Γ_1	0.75
Overlap integral (2300 nm wave with doped core)	Γ_2	0.6
Fiber background loss at 793 nm	α_p	0.4 dB/m
Fiber background loss at 1960 nm	α_1	0.3 dB/m
Fiber background loss at 2300 nm	α_2	0.3 dB/m
Raman gain coefficient (for 2300 nm wave amplified by 1960 nm wave)	g_{R12}	$5 \times 10^{-4} (\text{W cm})^{-1}$
Reflection coefficient at 1960 nm at $z = 0$	R_{01}	0.99
Reflection coefficient at 1960 nm at $z = L$	R_{L1}	0.99
Reflection coefficient at 2300 nm at $z = 0$	R_{02}	0.99
Reflection coefficient at 2300 nm at $z = L$	R_{L2}	0.05 ... 0.9
Reflection coefficient at 793 nm at $z = L$	R_{Lp}	0.99

We numerically solved the system of Equations (8)–(10) with allowance for the boundary Conditions (12)–(16) using the iterative procedure based on the Runge–Kutta method [29]. Note that we did not consider additional effects that may limit the output power, except for those described in the numerical model.

3. Results

We performed a series of numerical simulations and optimizations using the developed model to demonstrate the main idea of this work. It may be formulated as the possibility of achieving efficient generation at the demanded wavelength of 2300 nm with efficiency significantly exceeding the Stokes limit with a 793 nm diode pump—specifically, in Tm-doped zinc-tellurite glass fibers. A quite unique combination of laser gain bands and the Raman band of the selected glass allows the implementation of dual-wavelength generation at 1960 nm and 2300 nm, with additional Raman energy transfer between laser waves dramatically increasing the efficiency for the 2300 nm wave. The Raman terms were included and omitted from Equations (8)–(10), aimed at revealing their influence on the total efficiency. The spectroscopic characteristics were taken from Table 1. The other parameters of the active zinc-tellurite fiber were taken from Table 2.

Figure 3a–c demonstrate examples of power distributions in waves at λ_p in the forward and backward directions P_p^+ , P_p^- , as well as the distributions of laser waves P_1^+ , P_1^- , P_2^+ , P_2^- along the active zinc-tellurite fiber with $L = 100 \text{ cm}$ at a pump power of 10 W and $R_{L02} = 0.5$, with and without allowance for the Raman interaction in Equations (8)–(10). The solid lines correspond to the complete model and the dashed lines to the model with the omission of terms responsible for the Raman effects. The pump wave evolution in Figure 3a demonstrates the independence of the pump distribution along the fiber on the presence and absence of Raman effects. The laser wave distribution strongly depends on the stimulated Raman scattering. Waves trapped in the cavity at 1960 nm in both directions in the absence of Raman effects would have average intracavity powers of more than 20 W, while Raman scattering into waves at 2300 nm leads to an order of magnitude decrease in the intracavity powers at 1960 nm (Figure 3b). At the same time, the allowance for the Raman amplification of the wave at 2300 nm due to the wave at 1960 nm leads to an increase in power by approximately a factor of two (Figure 3c).

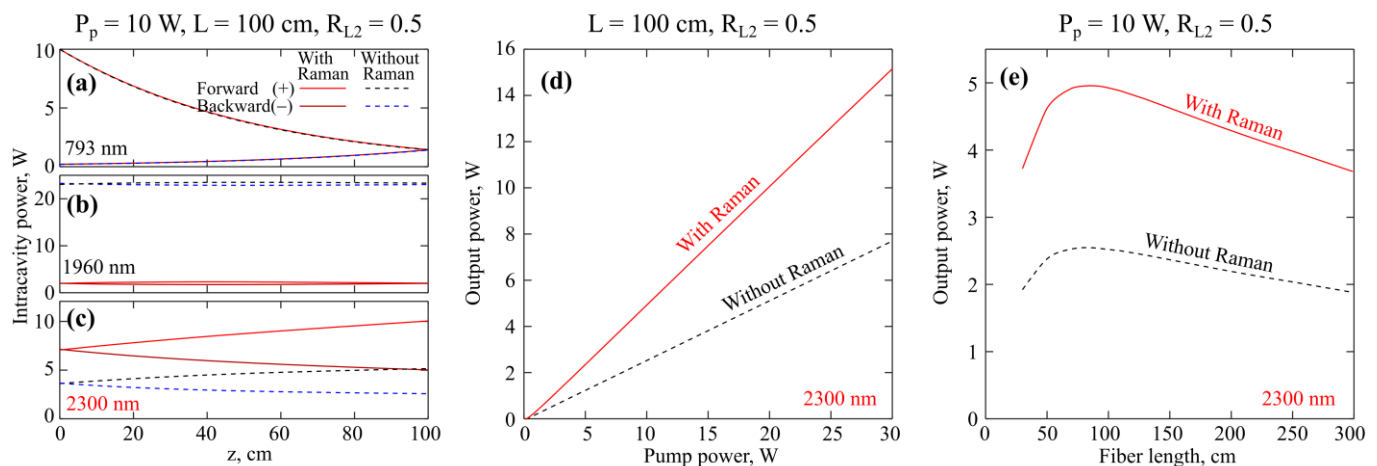


Figure 3. (a) Intracavity power evolution calculated for $P_p = 10$ W, $L = 100$ cm in the framework of the complete model with (solid lines) and without (dotted lines) Raman scattering for waves at 793 nm (a), 1960 nm (b) and 2300 nm (c). (d) Output power of the wave at 2300 nm as a function of pump power calculated with and without Raman gain for $L = 100$ cm. (e) Output power of the wave at 2300 nm as a function of fiber cavity length calculated with and without Raman gain for $P_p = 10$ W. $R_{L2} = 0.5$ for all subplots.

Next, we simulated the dependence of the output power at 2300 nm on the pump power, also with and without Raman scattering, for $L = 100$ cm and $R_{L02} = 0.5$ (Figure 3d). It can be seen that the dependences are almost linear, and the slope efficiency with Raman scattering taken into account is $\sim 50\%$, while that without Raman scattering is half this value. It is important to emphasize that the efficient transfer of power from the wave at 1960 nm to the wave at 2300 nm due to Raman scattering results in the pronounced exceedance of the total conversion efficiency of the diode pump to the 2300 nm wave over the Stokes limit, which is approximately 35%.

Then, we fixed the pump power $P_p = 10$ W and performed simulations for lasers with different lengths of the intracavity active fiber (Figure 3e). The result was quite expected: there is an optimal length for which the highest power is achieved, and the maximum is rather smooth. Note that this tendency is characteristic of fiber lasers operating on radiative transitions of different rare-earth ions [30]. In this case, the power, with Raman interaction taken into account, is almost twice as high as without Raman scattering for any L .

Next, we investigated the effects of the reflection coefficient R_{L2} on the efficiency of pump conversion to the laser wave at 2300 nm. The output laser power as a function of the pump power is plotted in Figure 4a,b. Figure 4a represents the trends at high powers, and Figure 4b shows the same curves but at low powers to mark the laser thresholds. At high powers, the dependences are almost linear, with slope efficiency of over 50% being achieved at $R_{L2} \leq 0.5$. The highest efficiencies of approximately 57% are obtained at $R_{L2} = 0.05\text{--}0.1$. The larger R_{L2} , the lower the lasing thresholds, as can be clearly seen in Figure 4b and as follows from the general theory of lasers [27]. Thus, at $R_{L2} = 0.9, 0.5, 0.1$ and 0.05 , the threshold pump powers are approximately equal to 80 mW, 200 mW, 600 mW and 700 mW, respectively. Thus, Figure 4 demonstrates that if the goal is to build a laser with a power of approximately 10 W, then it is better to use reflective structures at the output end with a low coefficient $R_{L2} \leq 0.3$, and an optimum of approximately $R_{L2} \sim 0.1$ can be achieved even due to the Fresnel reflection from the end of the Tm-doped zinc-tellurite fiber. Further, in our problem for target laser powers at 2300 nm of tens of mW, it is better to use high reflection coefficients $R_{L2} \geq 0.5$. For target laser powers of hundreds of mW, intermediate reflection coefficients should be chosen in the range from ~ 0.3 to ~ 0.7 . Moreover, $R_{L2} \sim 0.5$ is a fairly universal value that makes it possible to obtain sufficiently high efficiencies even at pump powers of hundreds of mW.

and, at the same time, provides high (albeit not maximum) efficiencies with a pump power of tens of W.

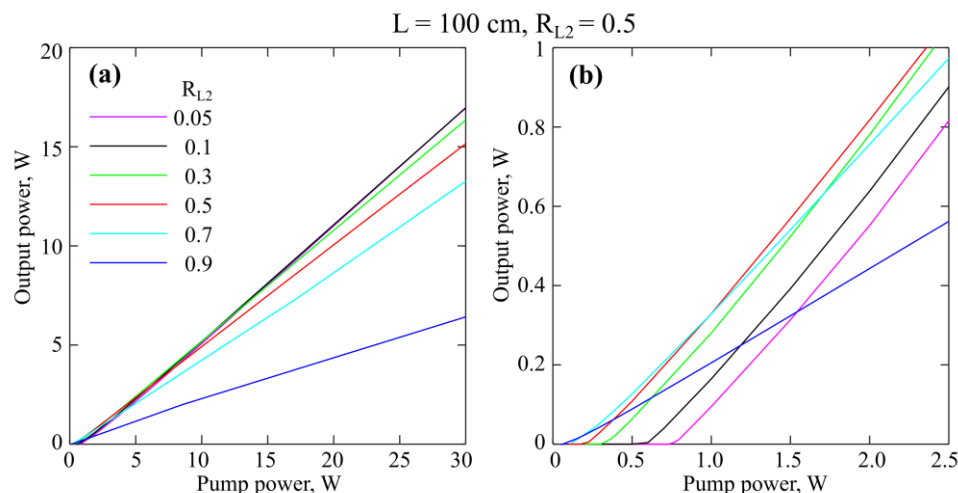


Figure 4. Output power of the wave at 2300 nm vs. pump power calculated for $L = 100$ cm and different R_{L2} . Graphs in (a,b) correspond to the same data but on a magnified scale for (b). The legends for (a,b) are the same.

We also examined the system variability in terms of choosing the active fiber length. In the real experiments, some differences from the simulation predictions could be observed—for example, due to inaccurately known parameters or unaccounted for minor effects. However, general dependences tend to persist. The numerically simulated laser output powers at 2300 nm as a function of L are plotted in Figure 5 for different R_{L2} at a fixed pump power of 10 W. It is seen that the maxima are not sharp; for a small $R_{L2} \sim 0.05$ – 0.1 , providing the highest efficiency, the curves are the smoothest. Thus, when choosing an optimal fiber length, one may make a mistake by more than two times (take L in the range from <1 m to >2 m), while the conversion efficiency will not change significantly. However, with an increase in R_{L2} , the maxima in Figure 5 become sharper, which means that for $R_{L2} > 0.5$, the choice of length should be made more carefully.

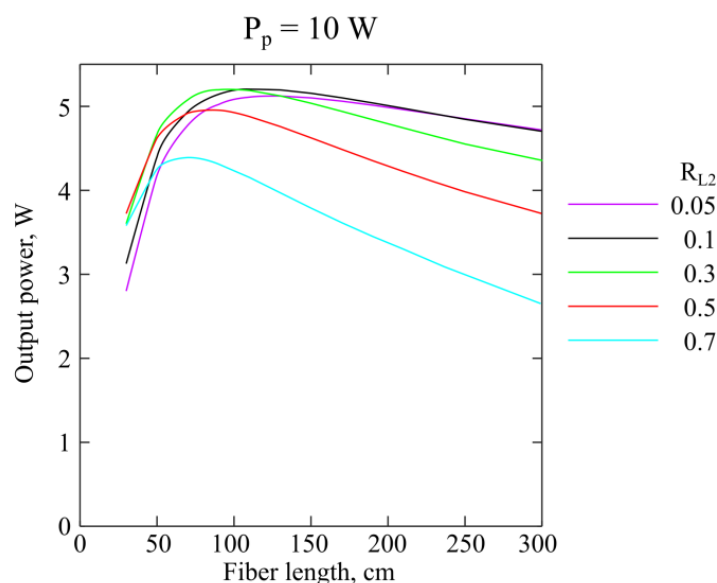


Figure 5. Output power of the wave at 2300 nm vs. fiber cavity length calculated for $P_p = 10$ W and different R_{L2} .

Finally, we investigated the effect of the fiber background loss on the quantitative characteristics of lasing at 2300 nm. For all the simulations presented above, we assumed a background optical loss of 0.4 dB/m at the pump wavelength and 0.3 dB/m at laser wavelengths. We considered cases when these values are various multiples of times ($\times 2$, $\times 3$, $\times 4$ and $\times 5$). For example, “ $\times 3$ ” means that the losses are 1.2 dB/m at 793 nm and 0.9 dB/m at 1960 and 2300 nm. The calculated output powers at 2300 nm vs. the length of the active fiber L at a fixed pump power of 10 W and the reflection coefficient $R_{L2} = 0.1$ are plotted in Figure 6. It is seen that although the losses affect both the maximum output powers and the optimal lengths, this effect is not critical. Thus, with an increase in background losses by a factor of 5, the maximum power is halved. At the same time, with increasing losses, the optimal lengths decrease, and the maxima become sharper, which is quite expected. The main conclusion from this series of simulations is that low optical losses are not a critical condition for the implementation of 2300 nm lasers with a watt power level, and this technology can be made available for many scientific labs.

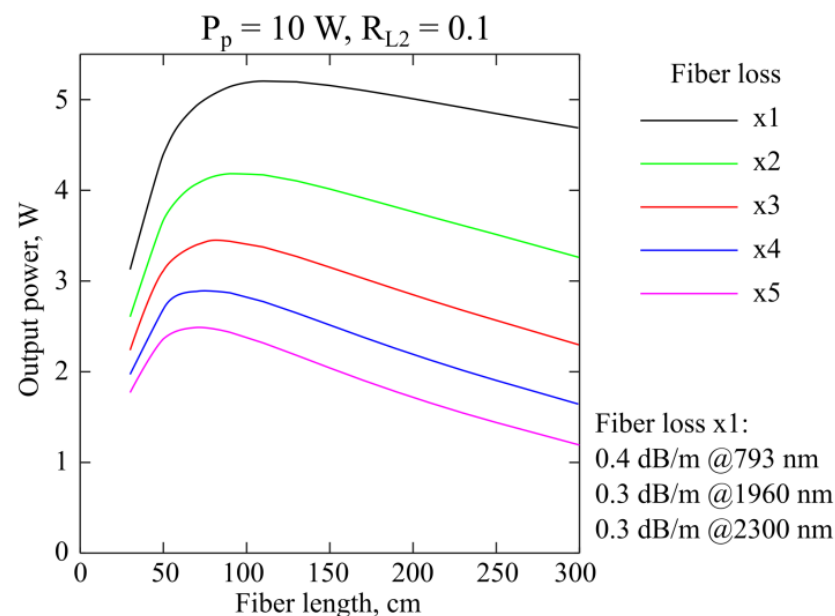


Figure 6. Output power of the wave at 2300 nm as a function of fiber cavity length calculated for $P_p = 10$ W, $R_{L2} = 0.1$ and different values of background fiber losses.

4. Discussion and Conclusions

We have proposed and theoretically studied a highly efficient Tm-doped zinc-tellurite fiber laser operating at two cascade ${}^3\text{H}_4 \rightarrow {}^3\text{H}_5$ and ${}^3\text{F}_4 \rightarrow {}^3\text{H}_6$ radiative transitions at 2300 nm and 1960 nm, respectively, with additional Raman interaction between the generated waves. A commercially available multimode laser diode at 793 nm was taken as a pump source. The numerical simulations showed that a dramatic increase in the slope efficiency for the laser wave at 2300 nm can be achieved thanks to the Raman energy transfer from the wave at 1960 nm to the wave at 2300 nm. The choice of zinc-tellurite glass was explained by the high Raman gain at a frequency of ~ 22.5 THz equal to the frequency difference between the laser waves. For the optimized parameters ($L \sim 100$ cm and output reflection coefficient of approximately 0.05–0.1), 10 W class fiber lasers with slope efficiency of up to 57%, exceeding the Stokes limit by 22%, were demonstrated. We also studied the impact of increased background losses on the output laser power at 2300 nm. It was shown that low optical losses are not a critical condition for the implementation of 2300 nm lasers with a multi-watt power level.

Author Contributions: Conceptualization, E.A.A.; methodology, E.A.A.; software, E.A.A.; validation, E.A.A. and A.V.A.; formal analysis, E.A.A. and A.V.A.; investigation, E.A.A.; data curation, E.A.A.; writing—original draft preparation, E.A.A.; writing—review and editing, A.V.A.; visualization, E.A.A. All authors have read and agreed to the published version of the manuscript.

Funding: The work was supported in part by the Center of Excellence “Center of Photonics” funded by the Ministry of Science and Higher Education of the Russian Federation, contract No. 075-15-2022-316 (investigation of highly efficient generation), and in part by the Ministry of Science and Higher Education of the Russian Federation, state assignment for the Institute of Applied Physics RAS, project FFUF-2021-0012 (development of numerical model).

Data Availability Statement: Data underlying the results presented in this article may be obtained from the authors upon reasonable request.

Conflicts of Interest: The authors declare no conflict of interest.

References

- Wang, Z.; Zhang, B.; Liu, J.; Song, Y.; Zhang, H. Recent developments in mid-infrared fiber lasers: Status and challenges. *Opt. Laser Technol.* **2020**, *132*, 106497. [\[CrossRef\]](#)
- Liu, H.; Yu, Y.; Song, W.; Jiang, Q.; Pang, F. Recent development of flat supercontinuum generation in specialty optical fibers. *Opto-Electron. Adv.* **2019**, *2*, 180020. [\[CrossRef\]](#)
- Soboń, G.; Lindberg, R.; Pasiskevicius, V.; Martynkien, T.; Sotor, J. Shot-to-shot performance analysis of an all-fiber supercontinuum source pumped at 2000 nm. *J. Opt. Soc. Am. B* **2018**, *36*, A15–A21. [\[CrossRef\]](#)
- Chen, L.; Liao, M.; Bi, W.; Yu, F.; Wang, T.; Gao, W.; Hu, L. Coherent Supercontinuum Generation in Step-Index Heavily Ge-Doped Silica Fibers with All Normal Dispersion. *IEEE Photonics J.* **2022**, *14*, 1–6. [\[CrossRef\]](#)
- Zhluktova, I.V.; Kamynin, V.A.; Korobko, D.A.; Abramov, A.S.; Fotiadi, A.A.; Sysoliatin, A.A.; Tsvetkov, V.B. Broadband Supercontinuum Generation in Dispersion Decreasing Fibers in the Spectral Range 900–2400 nm. *Photonics* **2022**, *9*, 773. [\[CrossRef\]](#)
- Fortin, V.; Bernier, M.; Faucher, D.; Carrier, J.; Vallée, R. 37 W fluoride glass Raman fiber laser operating at 2231 nm. *Opt. Express* **2012**, *20*, 19412–19419. [\[CrossRef\]](#)
- Jiao, Y.; Jia, Z.; Guo, X.; Zhao, Z.; Ohishi, Y.; Qin, W.; Qin, G. Third-order cascaded Raman shift in all-solid fluorotellurite fiber pumped at 1550 nm. *Opt. Lett.* **2022**, *47*, 690–693. [\[CrossRef\]](#)
- Yao, T.; Huang, L.; Zhou, P.; Lei, B.; Leng, J.; Chen, J. Power scaling on tellurite glass Raman fibre lasers for mid-infrared applications. *High Power Laser Sci. Eng.* **2018**, *6*, e24. [\[CrossRef\]](#)
- Vasilyev, S.; Moskalev, I.; Mirov, M.; Mirov, S.; Gapontsev, V. Multi-Watt mid-IR femtosecond polycrystalline Cr²⁺:ZnS and Cr²⁺:ZnSe laser amplifiers with the spectrum spanning 20–26 μ m. *Opt. Express* **2016**, *24*, 1616–1623. [\[CrossRef\]](#)
- Allen, R.; Esterowitz, L. cw diode pumped 2.3 μ m fiber laser. *Appl. Phys. Lett.* **1989**, *55*, 721. [\[CrossRef\]](#)
- Tyazhev, A.; Starecki, F.; Cozic, S.; Loiko, P.; Guillemot, L.; Braud, A.; Joulain, F.; Tang, M.; Godin, T.; Hideur, A.; et al. Watt-level efficient 2.3 μ m thulium fluoride fiber laser. *Opt. Lett.* **2020**, *45*, 5788–5791. [\[CrossRef\]](#)
- Falconi, M.C.; Laneve, D.; Prudenzano, F. Advances in Mid-IR Fiber Lasers: Tellurite, Fluoride and Chalcogenide. *Fibers* **2017**, *5*, 23. [\[CrossRef\]](#)
- Anashkina, E.A. Laser Sources Based on Rare-Earth Ion Doped Tellurite Glass Fibers and Microspheres. *Fibers* **2020**, *8*, 30. [\[CrossRef\]](#)
- Muravyev, S.V.; Anashkina, E.A.; Andrianov, A.V.; Dorofeev, V.V.; Motorin, S.E.; Koptev, M.Y.; Kim, A.V. Dual-band Tm³⁺-doped tellurite fiber amplifier and laser at 1.9 μ m and 2.3 μ m. *Sci. Rep.* **2018**, *8*, 16164. [\[CrossRef\]](#)
- Denker, B.I.; Dorofeev, V.V.; Galagan, B.I.; Koltashev, V.V.; Motorin, S.E.; Plotnichenko, V.G.; Sverchkov, S.E. A 200 mW, 2.3 μ m Tm³⁺-doped tellurite glass fiber laser. *Laser Phys. Lett.* **2020**, *17*, 095101. [\[CrossRef\]](#)
- Kamynin, V.; Filatova, S.; Denker, B.; Galagan, B.; Koltashev, V.; Medvedkov, O.; Sverchkov, S.; Tsvetkov, V. Tm³⁺-doped tellurite fiber weak signal amplifier at a wavelength of 2.27 μ m. *Results Phys.* **2021**, *27*, 104512. [\[CrossRef\]](#)
- Koptev, M.Y.; Anashkina, E.A.; Andrianov, A.; Muravyev, S.V.; Kim, A. Two-color optically synchronized ultrashort pulses from a Tm/Yb-co-doped fiber amplifier. *Opt. Lett.* **2014**, *39*, 2008–2011. [\[CrossRef\]](#)
- Wu, Y.; Yao, C.; Wang, C.; Yang, L.; Wang, X.; Ren, G.; Li, P. High-Energy 1.96–2.4 μ m Tunable Raman Soliton Generation in All-Silica-Fiber Tm-Doped Amplifier. *IEEE Photonics Technol. Lett.* **2023**, *35*, 361–364. [\[CrossRef\]](#)
- Dvoyrin, V.V.; Turitsyn, S.K. Generation of high-energy soliton-like pulses in 1.9–2.5 μ m spectral domain. *J. Phys. Photonics* **2020**, *2*, 044005. [\[CrossRef\]](#)
- Kirsch, D.C.; Bednyakova, A.; Varak, P.; Honzatko, P.; Cadier, B.; Robin, T.; Fotiadi, A.; Peterka, P.; Chernysheva, M. Gain-controlled broadband tuneability in self-mode-locked Thulium-doped fibre laser. *Commun. Phys.* **2022**, *5*, 219. [\[CrossRef\]](#)
- Jackson, S.D.; Mossman, S. Efficiency dependence on the Tm³⁺ and Al³⁺ concentrations for Tm³⁺-doped silica double-clad fiber lasers. *Appl. Opt.* **2003**, *42*, 2702–2707. [\[CrossRef\]](#)
- Aydın, Y.O.; Fortin, V.; Maes, F.; Jobin, F.; Jackson, S.D.; Vallée, R.; Bernier, M. Diode-pumped mid-infrared fiber laser with 50% slope efficiency. *Optica* **2017**, *4*, 235–239. [\[CrossRef\]](#)

23. Plotnichenko, V.G.; Sokolov, V.O.; Koltashev, V.V.; Dianov, E.M.; Grishin, I.A.; Churbanov, M.F. Raman band intensities of tellurite glasses. *Opt. Lett.* **2005**, *30*, 1156–1158. [[CrossRef](#)]
24. Gomes, L.; Lousteau, J.; Milanese, D.; Scarpignato, G.C.; Jackson, S.D. Energy transfer and energy level decay processes in Tm^{3+} -doped tellurite glass. *J. Appl. Phys.* **2012**, *111*, 063105. [[CrossRef](#)]
25. Rhonehouse, D.L.; Zong, J.; Nguyen, D.; Thapa, R.; Wiersma, K.; Smith, C.; Chavez-Pirson, A. Low loss, wide transparency, robust tellurite glass fibers for mid-IR (2–5 μm) applications. *SPIE Proc.* **2013**, *8898*, 88980D. [[CrossRef](#)]
26. Evrard, M.; Combes, T.; Maldonado, A.; Désévéday, F.; Gadret, G.; Strutyński, C.; Jules, J.C.; Brachais, C.H.; Smektala, F. TeO_2 - ZnO - La_2O_3 tellurite glass purification for mid-infrared optical fibers manufacturing. *Opt. Mater. Express* **2021**, *12*, 136–152. [[CrossRef](#)]
27. Svelto, O.; Hanna, D.C. *Principles of Lasers*; Springer: New York, NY, USA, 2010.
28. Agrawal, G.P. *Nonlinear Fiber Optics*, 6th ed.; Elsevier: Amsterdam, The Netherlands, 2019.
29. Jackson, S.D.; Muir, P.H. Theory and numerical simulation of nth-order cascaded Raman fiber lasers. *J. Opt. Soc. Am. B* **2001**, *18*, 1297–1306. [[CrossRef](#)]
30. Sojka, L.S.; Tang, Z.; Zhu, H.; Bereś-Pawlik, E.; Furniss, D.; Seddon, A.; Benson, T.M.; Sujecki, S. Study of mid-infrared laser action in chalcogenide rare earth doped glass with Dy^{3+} , Pr^{3+} and Tb^{3+} . *Opt. Mater. Express* **2012**, *2*, 1632–1640. [[CrossRef](#)]

Disclaimer/Publisher’s Note: The statements, opinions and data contained in all publications are solely those of the individual author(s) and contributor(s) and not of MDPI and/or the editor(s). MDPI and/or the editor(s) disclaim responsibility for any injury to people or property resulting from any ideas, methods, instructions or products referred to in the content.